Batteries & Supercaps

Research Article
doi.org/10.1002/batt.202400250

Chemistry Europe
European Chemical Societies Publishing

www.batteries-supercaps.org

Nucleation Mechanisms of Electrodeposited Magnesium on Metal Substrates

Mario Löw[+],[a] Fabio Maroni[+],[a] Steve Zaubitzer,[a] Saustin Dongmo,[a] and Mario Marinaro*[a, b]

Magnesium rechargeable batteries (RMBs) are a promising alternative to lithium-based ones. However, a major challenge in their advance concerns the development of aprotic electrolytes from which magnesium can be electrodeposited with high efficiency and without the formation of dendrites. Of note, the mechanism of the magnesium electrodeposition from aprotic electrolytes remains largely unexplored. In this study, we propose a combined experimental and theoretical approach based on the Scharifker-Hills (S–H) mathematical model for the potentiostatic transients to analyse the nucleation and growth of magnesium during electrodeposition in order to shed light on the nucleation process and increase battery safety and cycle lifetime. The model is used to investigate the electrodeposition of magnesium from a Magnesocene ($MgCp_2$)-based electrolyte onto metal current substrates such as copper, nickel, aluminium and stainless steel.

Introduction

The rise of renewable, green energy sources, the trend towards the decarbonisation of society, and an increasing demand for electric cars have led to a higher demand for energy storage systems.[1–4] Since their introduction in the early 1990s, Lithium-ion batteries (LiBs) have been the technology of choice for high-demand applications.[5,6] However, LiBs face some downsides regarding the abundance of lithium and its cost compared to magnesium. Lithium has an abundance of 20 parts per million (ppm) in the earth's crust, whereas magnesium has 23300 ppm. This higher abundance also significantly affects the price of the two raw materials with only 0.26 USD per gram for magnesium but 1.44 USD per gram for lithium.[7] Considering Rechargeable Magnesium Batteries (RMB) as an alternative to lithium ion batteries is not limited to their economic advantages alone.[8,9] For instance, magnesium offers higher volumetric capacity than lithium (3833 $mAh\,cm^{-3}$ vs. 2061 $mAh\,cm^{-3}$) and a comparatively low potential of 2.37 V vs. SHE. However, a few roadblocks still hinder the full exploitation of RMBs. For instance, cathode materials having high capacities, fast kinetics, long cycle life and operating at high potentials need further development.[10,11]

Moreover, one of the many drawbacks RMBs face, occurs at the magnesium anode/ aprotic electrolyte interface, where intense research has been ongoing in recent times.[12–16] One of the challenges there, and in general with all metal anode batteries, is the formation of dendrites, but also the formation of a passivation layer due to the very negative standard potential of alkali- and alkali-earth-metals.[17–25] However, the formation of dendrites happens for RMBs only under certain conditions.[26–29]

To understand the electro-plating of magnesium, it is essential to understand the nucleation behaviour since this is the initial point of the metal deposition. However, magnesium's electrodeposition and nucleation mechanisms in aprotic electrolytes remain largely unexplored.[30,31] Therefore, this work aims to combine experimental and mathematical approaches to understand the nucleation and growth mechanism of Mg metal deposition from chronoamperometry *i–t* measurements. The magnesium nucleation behaviour is analysed with a mathematical model based on the Scharifker and Hills theory.[32] These techniques have been used numerous times to investigate the nucleation and growth behaviour of most diverse metals including lithium.[33–38]

Herein, a halogen-free Magnesocene-based model electrolyte developed and investigated by Schwarz and co-workers has been used.[25,39, 40] The electrolyte shows good long-term cycling performance (500 cycles) and high columbic efficiency of up to 98%. Moreover, magnesium can be electrodeposited without any evidence of electrolyte degradation.[25] Theoretical calculations show that the $MgCp_2THF_2$ species is the most stable in the solution. Since the cathodic stability of $MgCp_2THF_2$ is located well below 0 V vs. Mg/Mg^{2+}, no passivation layer is forming on the surface during electrodeposition, which could block stripping and plating processes.[39]

This work investigates the electrochemical and the nucleation behaviour of Mg in the $MgCp_2$ electrolyte on different metal substrates like copper (Cu), nickel (Ni), aluminium (Al), stainless steel ($FeCr_{18}Ni_{10}Mo_3$) (SS) at different selected potential values.

[a] M. Löw,[+] Dr. F. Maroni,[+] Dr. S. Zaubitzer, Dr. S. Dongmo, Dr. M. Marinaro
Zentrum für Sonnenenergie-und Wasserstoff-Forschung Baden-Württemberg, Helmholtzstraße 8, 89081 Ulm
E-mail: mario.marinaro@zsw-bw.de

[b] Dr. M. Marinaro
Present address: Institute of Theoretical Chemistry, Universität Ulm, Lise-Meitner-Straße 16, 89081 Ulm

[+] The authors equally contributed for first authorship.

Supporting information for this article is available on the WWW under https://doi.org/10.1002/batt.202400250

Research Article
doi.org/10.1002/batt.202400250
Chemistry Europe
European Chemical Societies Publishing

Results and Discussion

Nucleation and Growth of Magnesium

To understand the electrochemically driven Mg nucleation mechanism on different metal substrates, chronoamperometry (CA) is a very useful technique, followed by the application of a well-known mathematical model, the Scharifker-Hills model (S–H Model) .[32] Therefore, the potential of the metal substrates was set to six different values, namely $E=-0.100$ V (vs. Mg/Mg^{2+}), $E=-0.350$ V (vs. Mg/Mg^{2+}), $E=-0.500$ V (vs. Mg/Mg^{2+}) $E=-0.750$ V (vs. Mg/Mg^{2+}), $E=-1.000$ V (vs. Mg/Mg^{2+}) and $E=-1.250$ V (vs. Mg/Mg^{2+}), respectively. From the current-time transient, the nucleation mechanisms were then investigated, by elaborating raw data into a theoretical-curves fit, following the model developed by Scharifker and Hills.[32,33] Briefly, the model considers hemispherical nucleation centres that grow with time and overlap reaching a maximum current that approaches a limit value, finally reaching a planar diffusion behaviour. These considerations are applied to the current-time transients during a chronoamperometric experiment, as it is shown in Figure 1. The curve can be divided into four different segments, labelled as I, II, III and IV respectively. These processes are sensible and can be quite fast. For this reason, recording correctly an experiment requires a careful setting of the cell setup and speed of data sampling.

The first segment (I), in the green section of the plot, at the beginning of the measurement, corresponds to double-layer charging.[33] This process is usually very fast. In the second section (labelled as II, in violet), the current increases because of the progressive electroactive surface area growth.[41] This increase in surface area can occur following two different pathways: the first one is a rather isolated and fast early stage growth of nuclei, which corresponds to a so-called instantaneous nucleation mechanism. The second pathway involves a slower nucleation rate of the total number of deposited metal nuclei, which continues, at a later stage, during nuclei growth, with a so-called progressive nucleation mechanism. In short, on the one hand, when the nucleation rate (r_{nucl}) is much higher of the nuclei growth rate (r_{growth}), $r_{nucl} \gg r_{growth}$, we are in presence of a 3D-instantaneous mechanism. On the other hand when $r_{nucl} \sim r_{growth}$, the mechanism is progressive.

During this phase, the overlapping of the nuclei does not play a role. Looking then at the orange section, labelled as III in Figure 1, growth of independent nuclei and nuclei overlap occur simultaneously: the current density first increases until it reaches a maximum and then it declines again. In the last section, labelled as IV (light blue), which is located behind the t_{max}-value, the growth of Mg-nuclei is controlled by linear diffusion to the electrode surface and the current starts to decrease because of the decreased active surface.

By knowing t_{max}, j_{max} and the values for t and j of the current-time-transient, it is possible to determine the nucleation mechanism with a dimensionless mathematical model derived by Scharifker and Hills. The equations for this model, for the two different nucleation mechanisms – instantaneous and progressive – are shown below:[32,42]

Instantaneous nucleation:[32,34,42]

$$\frac{j^2}{j_{max}^2} = 1.9542 \cdot \left(\frac{t_{max}}{t}\right) \cdot \left[1 - exp\left(-1.2564 \cdot \frac{t}{t_{max}}\right)\right]^2 \quad (1)$$

Progressive nucleation:[32,34,42]

$$\frac{j^2}{j_{max}^2} = 1.2254 \cdot \left(\frac{t_{max}}{t}\right) \cdot \left[1 - exp\left(-2.3367 \cdot \frac{t^2}{t_{max}^2}\right)\right]^2 \quad (2)$$

Here, j is the current density, j_{max} is the maximum of the current density, t is time, t_{max} is the time at the current density maximum.

Further, an important aspect of the S–H model is finding diagnostic criteria that can help in acknowledging its applicability and consistency over several potential values, in chronoamperometric experiments. Scharifker and Hills, in their model development, found that the $(j_{max})^2 * t_{max}$ value can be used to that aim as it does not involve, in its mathematical expression, parameters like the steady state nucleation rate constant A, and the number density of active sites (N). In detail, the expressions are shown in eq. (3) and eq. (4):

$$(j_{max})^2 * t_{max} = 0.1629(zFc)^2 D \text{ 3D-Instantenous nucleation mechanism} \quad (3)$$

$$(j_{max})^2 * t_{max} = 0.2598(zFc)^2 D \text{ 3D-Progressive nucleation mechanism} \quad (4)$$

in which, z is the charge number, F is the Faraday constant, c is the concentration and D is the diffusion coefficient.

In Table 1, several $t_{max} * (j_{max})^2$ values are reported, for selected E (V vs. Mg/Mg^{2+}) values as well as for the selected metal substrates investigated in this paper. For sake of clarity on data handling, the obtained chronoamperometric J vs. t

Table 1. Summary of $t_{max} * (j_{max})^2$ values as requirement for the applicability of the S–H Method. $Mg(Cp)_2$ 0.05 M//THF electrolyte solution.

Potential (vs. Mg/Mg^{2+})	Cu	Ni	Al	SS
$E=-0.350$ V	$1.28*10^{-9}$	$1.93*10^{-9}$	–	$2.77*10^{-9}$
$E=-0.500$ V	$1.18*10^{-9}$	$1.33*10^{-9}$	$9.10*10^{-10}$	$1.97*10^{-9}$
$E=-0.750$ V	$1.63*10^{-9}$	$1.58*10^{-9}$	$8.27*10^{-9}$	$1.62*10^{-9}$
$E=-1.000$ V	$7.18*10^{-9}$	$2.11*10^{-9}$	$5.33*10^{-9}$	$1.52*10^{-9}$
$E=-1.250$ V	$3.87*10^{-9}$	$1.88*10^{-9}$	$1.521*10^{-8}$	$1.32*10^{-9}$

Research Article
doi.org/10.1002/batt.202400250
Chemistry Europe
European Chemical Societies Publishing

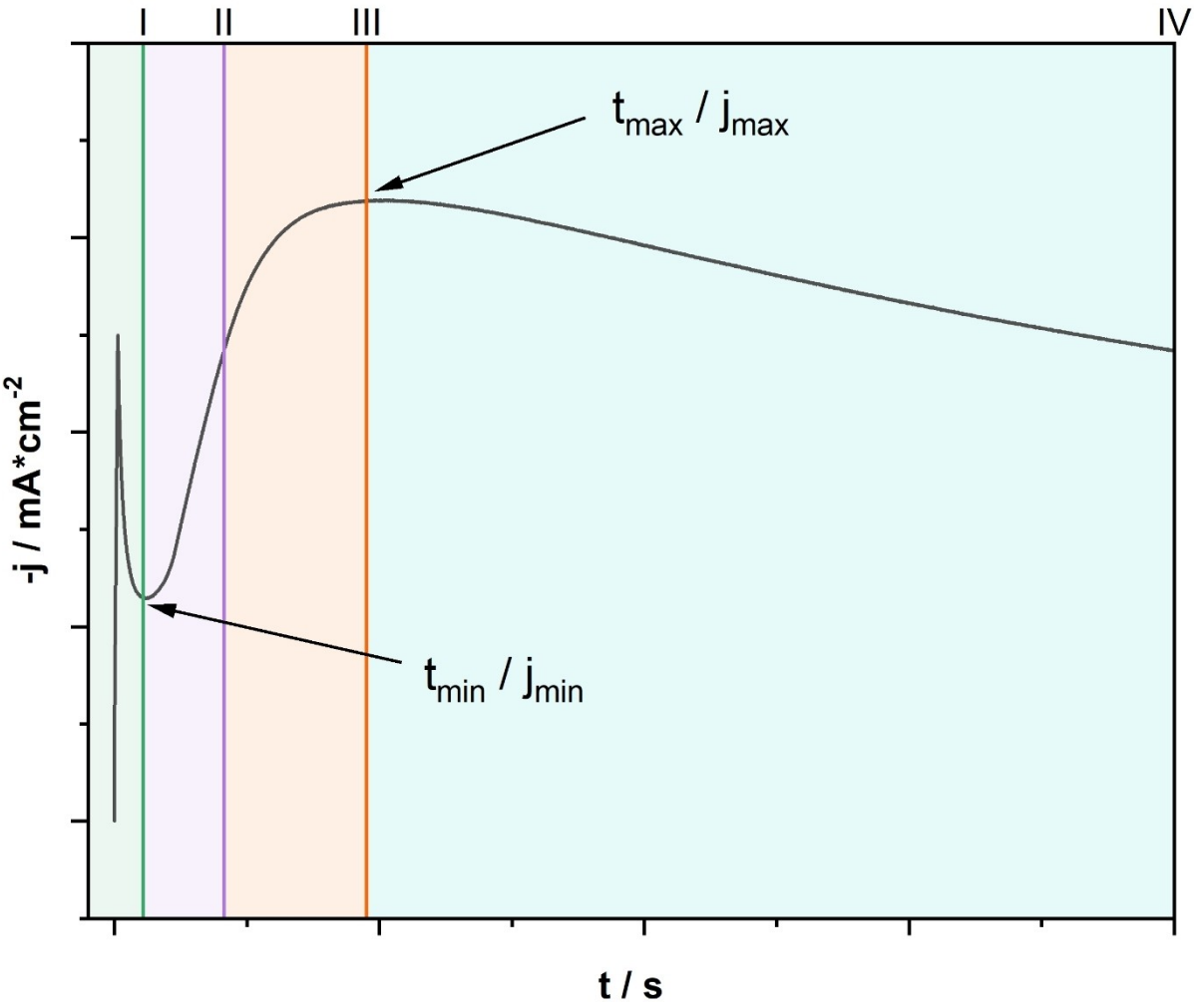

Figure 1. Current density-time transient, pointing out the position of j_{max} and t_{max}, the position of the double layer charging and the part two (blue), three (orange) and four (green) of the nucleation process.

plots were handled as follows: t_{min}/j_{min} values were identified (as can be seen in Figure 1), subtracted so that the plots are offset to 0. Then the j/t values progression have been evaluated. This is needed, because the initial phase of the experiment, involving the charging of the electrode double layer interface does not contain useful information.[43]

As it can be seen, for all the selected metal substrates, except Al which showed more deviations, the $t_{max}*(j_{max})^2$ values are very close to each other. It is worth noting, that to the best of our knowledge, this is the first application of the S–H model to the nucleation of magnesium from a non-aqueous solution. For this reason, we chose the order of magnitude as single approximation for the $t_{max}*(j_{max})^2$ evaluation. Anyway, the values in Table 1 show a strong consistency over a wide range of experiments.

Figure 2 shows the current-time profiles for the measured potential of the Mg deposition onto Cu from a 0.05 M $MgCp_2$/THF solution. Here, except for the experiment carried out at E = −0.100 V (vs. Mg/Mg^{2+}), all curves have the features explained in Figure 1. Additionally, the curves follow two trends. On one side, j_{max} increases with more a negative potential value. At more negative potentials, the nucleus density increases, which leads to a larger electroactive area.[33] On the other side, t_{max} decreases with more negative potential. This decrease of t_{max} values is caused by the activation energy for nucleation decreasing with more negative potential, facilitating the nucleation process.[33]

For sake of clarity, all the t_{max} and j_{max} values that confirm this statement are reported in Table 2, for a Cu substrate. All values concerning other metal substrates are reported in the supporting information. The applied potential value seems to have a generally determining effect over all the investigated metal substrates, in fact at E = −0.100 V (vs. Mg/Mg^{2+}) was not possible to apply the S–H model for any of the metal substrates.

Given the amount of experiments carried out and generated data, we here show results for the Cu substrate, while the discussion is generalized to the other metal substrates. The rest of the investigation data can be found in the Supporting Information. The experimental results for the Cu substrate, the dimensionless theoretical plots for the two types of nucleation

Research Article
doi.org/10.1002/batt.202400250
Chemistry Europe
European Chemical Societies Publishing

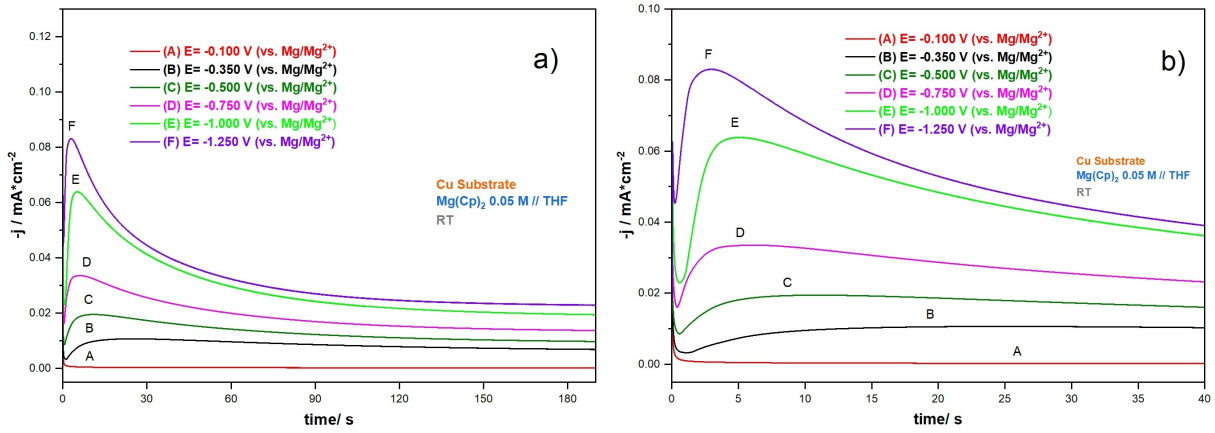

Figure 2. a) Current transient curves for Mg's electrochemical deposition on a Cu metal substrate at different potentials at a concentration of 0.05 M $MgCp_2$/THF; b) Detail of the early stage of the chronoamperometry experiment.

Table 2. Summary of t_{max}, j_{max} and $t_{max}*(j_{max})^2$ values for a Cu metal substrate. $Mg(Cp)_2$ 0.05 M/THF. The t_{max} and j_{max} values here reported are reported after offsetting to zero, the –j vs t plots by t_{min} and j_{min} subtraction.

Potential (vs. Mg/Mg^{2+})	Cu Substrate//$Mg(Cp)_2$ 0.05 M/THF		
	t_{max}/s	j_{max}/mA*cm^{-2}	$t_{max}*(j_{max})^2$
E = −0.100 V	–	–	–
E = −0.350 V	23.48	$7.39*10^{-3}$	$1.28*10^{-9}$
E = −0.500 V	10.01	$1.087*10^{-2}$	$1.18*10^{-9}$
E = −0.750 V	5.35	$1.744*10^{-2}$	$1.63*10^{-9}$
E = −1.000 V	4.29	$4.087*10^{-2}$	$7.18*10^{-9}$
E = −1.250 V	2.72	$3.772*10^{-2}$	$3.87*10^{-9}$

mechanisms, are plotted $(j/j_{max})^2$ against (t/t_{max}), according to the S–H model. The obtained results are shown in Figures 3.

In general for the Cu substrate, the 3D-Instantaneous mechanism has been found to be dominating at E = −0.350 V (vs Mg/Mg^{2+}) and E = −0.500 V (vs Mg/Mg^{2+}), E = −0.750 V (vs Mg/Mg^{2+}). Concerning E = −1.000 V (vs Mg/Mg^{2+}) and E = −1.250 V (vs Mg/Mg^{2+}), the fit is somewhat less clear, but the area of the curve close to the max seems to be still leaning towards a 3D-Instantaneous mechanism. This part of the curve is essential, because nucleation happens in this stage. Since the nuclei growth is controlled by linear diffusion to the surface of the electrode in the stage after the maximum, it is less important that the experimental curve fit the theoretical one in this area.

The same investigations were carried out on Al (Figure S1–S2), Ni (Figure S3–S4), SS (Figures S5–S6) substrates. Tables S1–S4 report the t_{max} and j_{max} values, as well as the $t_{max}*(j_{max})^2$ value for every applied potential. As result of this analysis, it turned out that on Ni and SS substrates, the Mg electrodeposition showed a clear indication of a 3D-Instantaneous nucleation mechanism for all the investigated potentials in which the S–H model has been found applicable, i.e. except E = −0.100 V (vs Mg/Mg^{2+}) in all cases. As it concerns Al, it showed the strongest substrate-potential dependence. While at E = −0.100 V (Vs. Mg/Mg^{2+}) and E = −0.350 V (Vs. Mg/Mg^{2+}) it was not even possible to find a real t_{max}/j_{max} couple, only at E = −0.750 V (Vs. Mg/Mg^{2+}) and E = −1.000 V (Vs. Mg/Mg^{2+}), the $t_{max}*(j_{max})^2$ value is consistent with the aforementioned diagnostic criterion for model applicability. At the former, Al did not show a clear mechanism to be assigned, while at the latter the fit with the theoretical curves is visibly leaning towards a 3D-Instantaneous mechanism. Further, it is worth noting, that at while E = −1.250 V (vs. Mg/Mg^{2+}) the $t_{max}*(j_{max})^2$ value is one order of magnitude greater, and so it would not be acceptable for model application with respect with the previous potential values, it shows anyway a very good theoretical curve fit with a 3D-Progressive nucleation mechanism. Speculatively, this could hint at an interplay of both potential and substrate dependence, which should be investigated more in detail near that potential value. Furthermore, we cannot completelly rule out the formation of an ultra-thin Mg-Al alloy. Phase diagramm for the binary Mg-Al alloys does exists. However, these alloys have only be obtained at very high temperature and there is, to the best of our knowledge, no report showing they can be also formed at room temperature. Finally, we could not see any indication from the electrochemical and analytical data of any Mg-Al alloys suggesting that, if formed, it must be of only few atoms thick. A summary of the obtained nucleation mechanisms as function of the set potential and of the metal substrate can be found in Table 3.

As a validation of the nucleation mechanism, post-mortem scanning electron microscopy (SEM) images of the Mg deposition on the investigated metal substrates from 0.05 M $MgCp_2$ at *E* = −1.000 V (vs. Mg/Mg^{2+}), were taken. The results for Cu and Ni are shown in Figure 4 and 5 respectively.

It is worth mentioning, that the deposition potential value, i.e. E = −1.000 V (vs. Mg/Mg^{2+}), was chosen because the $(j_{max})^2*t_{max}$ value is similar for all the experiments on various substrates, so that the model can be considered valid for all deposition experiments.

Figure 4 and Figure 5 show the deposition of Mg metal, at selected magnification values, on Cu and Ni substrates, respectively. Depositions conducted on SS and Al substrates

Research Article
doi.org/10.1002/batt.202400250
Chemistry Europe
European Chemical Societies Publishing

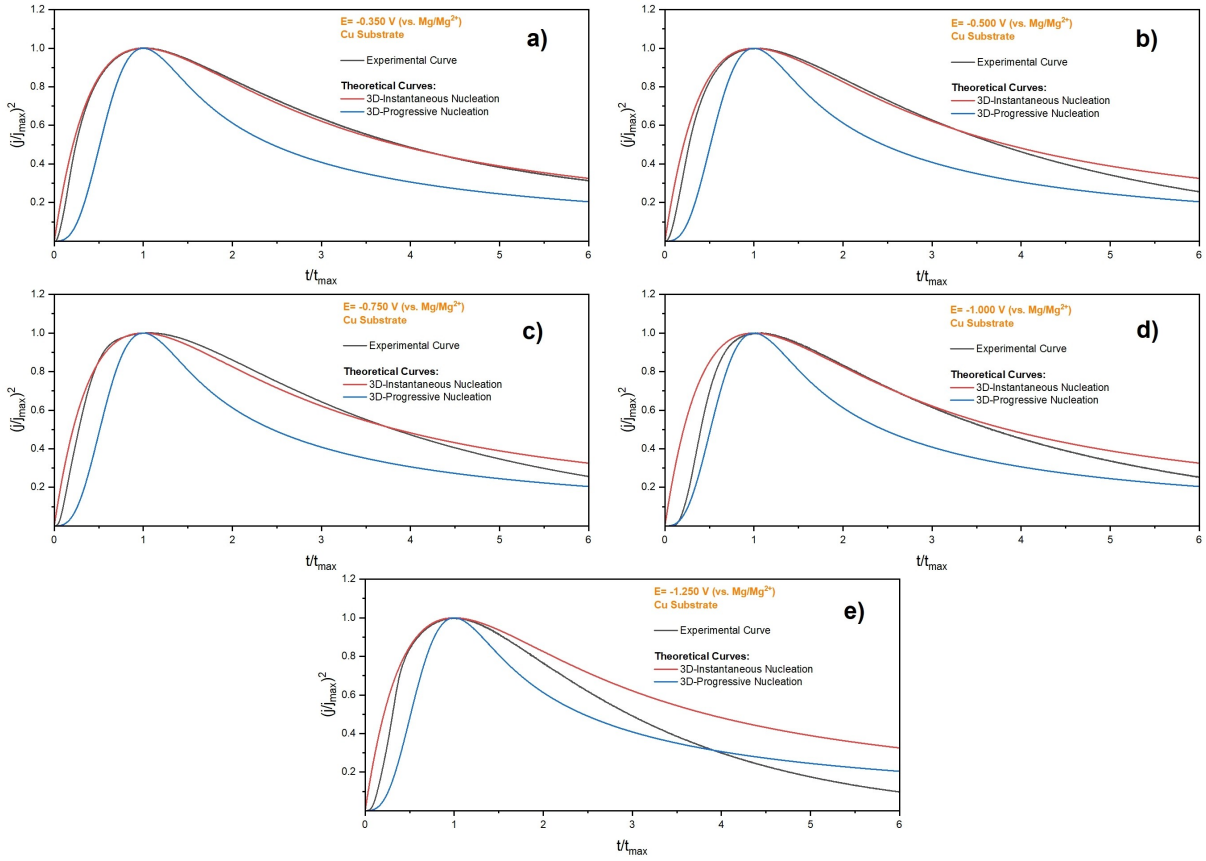

Figure 3. Scharifker & Hills analysis for the current-transient of magnesium electrodeposition on copper in 0.05 M $MgCp_2$ at a) E = −0.350 V (vs. Mg/Mg^{2+}), b) E = −0.500 V (vs. Mg/Mg^{2+}) c) E = −0.750 V (vs. Mg/Mg^{2+}) d) E = −1.000 V (vs. Mg/Mg^{2+}) and e) E = −1.250 V (vs. Mg/Mg^{2+}). Black curve is experimental data, Red curve is the S–H instantaneous theoretical plot and the Blue Curve is the S–H progressive nucleation theoretical plot.

Table 3. Nucleation mechanism summary for selected metal substrates at selected potential values.

Potential (vs. Mg/Mg^{2+})	Cu	Ni	Al	SS
E = −0.350 V	Instantaneous	Instantaneous	–	Instantaneous
E = −0.500 V	Instantaneous	Instantaneous	Not Applicable	Instantaneous
E = −0.750 V	Instantaneous	Instantaneous	Undecided	Instantaneous
E = −1.000 V	Undecided	Instantaneous	Instantaneous	Instantaneous
E = −1.250 V	Undecided (Leaning Instantaneous)	Instantaneous	Not Applicable	Instantaneous

can be found in SI. The experiments were recorded in a comparable time scale to the original nucleation experiments to keep reproducible conditions. In detail, calculations for the deposited amount of charge were done considering a theoretical uniform Mg-metal deposition thickness of 100 nm on the surface of the substrates. Energy Dispersive X-ray analysis (EDX), was conducted on selected spots of the electrode-deposited metal, to confirm the actual deposition. Results can be found in Supporting Information (Figure S9 and Table S3).

The first apparent aspect of the deposition is the influence of the metal substrate on particle shape. Bigger nuclei on Cu present a flower-like shape, while on Ni, the bigger Mg crystallites seem to have a more irregular and squared shape. Stainless steel, shows more regular hexagonal-shaped Mg-crystals, consistently with the actual hexagonal close packing (HCP) of bulk Mg-metal. Lastly, Al shows a very peculiar deposition shape with pillar-like aggregated particles.

The influence of the substrate is even more apparent when the theoretical curves fittings are taken into consideration. In detail, considering the E = −1.000 V (vs. Mg/Mg^{2+}) deposition potential, Ni and SS show a very good match with a purely instantaneous mechanism. Al is very close to a 3D-Instantaneous nucleation, while Cu substrate, as also reported in table 1, has been labelled as "Undecided" for a somewhat intermediate nature. When also the panoramic images, recorded a 500x are taken into consideration, the whole picture appears clearer. For a purely instantaneous nucleation mechanism, very well distributed small nuclei, across the substrate

Research Article
doi.org/10.1002/batt.202400250
Chemistry Europe
European Chemical Societies Publishing

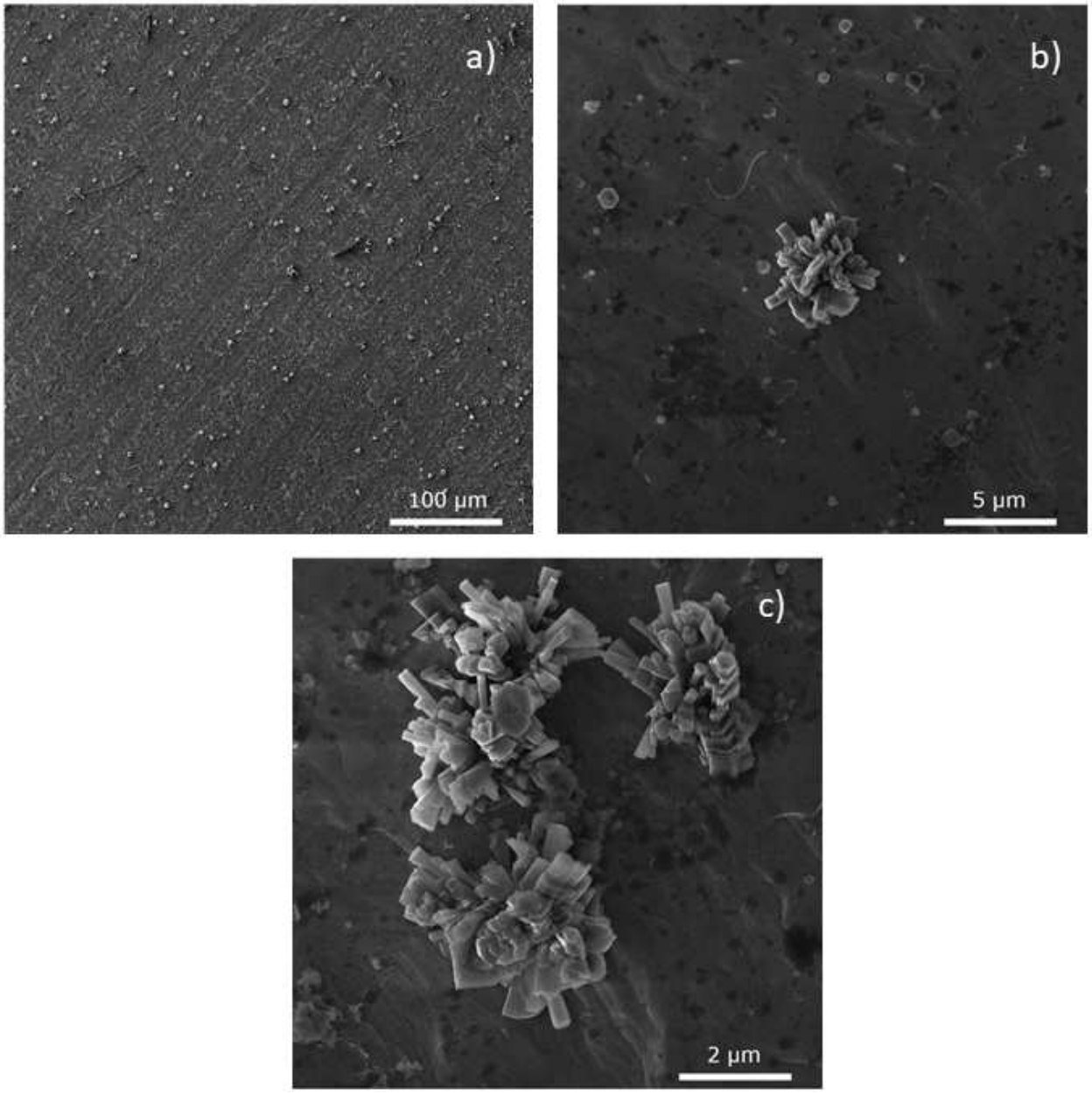

Figure 4. SEM image of magnesium plated on Cu, from a 0.05 M $MgCp_2$ in THF solution at $E = -1.000$ V vs. Mg/Mg^{2+} at selected magnifications: a) 500x, b) 10 Kx and c) 20 Kx.

surface can be detected, in Figure 5a (Ni) and S7a (SS), respectively. In fact, for this nucleation mechanism, $r_{nucl} \gg r_{growth}$ and all nuclei are formed simultaneously, and no new nuclei are formed. Thus, all nuclei should show similar size if there is instantaneous nucleation. Slightly departing from an almost ideal situation, as can be seen for Al, most of the nuclei are still very small, but an increased portion of the surface presents bigger aggregates. Lastly, for Cu, which has shown a more intermediate mechanism, the quota of bigger aggregates is even bigger. This could suggest a different balance for r_{nucl} and r_{growth}. Considering the same conditions in which the experiments were conducted and the results of the application of the mathematical model itself, experimental and theoretical data showed a very good degree of consistency and sensitivity.

As already shown in Eq. (3) and Eq. (4), the model developed by Scharifker and Hills also enables the determination of the diffusion coefficient of the Mg^{2+}-ion. The product for the t_{max} and j_{max} values $j^2_{max} \cdot t_{max}$ should be constant and independent from the applied potential. However, the diffusion coefficient is still dependent on the nucleation mechanism. Therefore, the diffusion coefficient can be obtained with the equations, for instantaneous, Eq. (5), and progressive nucleation, Eq. (6), respectively:[32,33,37]

Research Article
doi.org/10.1002/batt.202400250
Chemistry Europe
European Chemical Societies Publishing

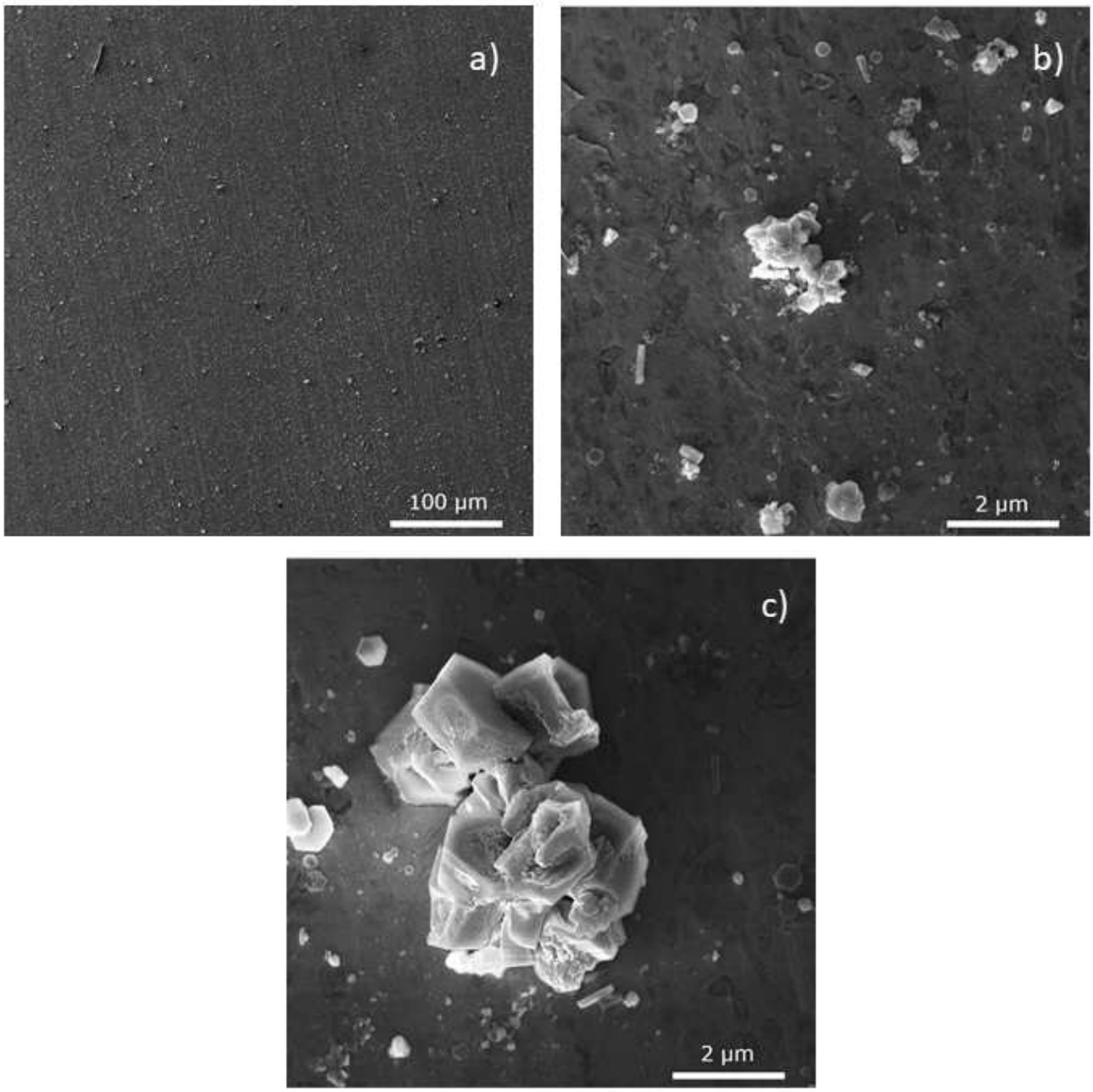

Figure 5. SEM image of magnesium plated on Ni, from a 0.05 M $MgCp_2$ in THF solution at $E = -1.000$ V vs. Mg/Mg^{2+} at selected magnifications: a) 500x, b) 20 Kx and c) 30 Kx.

$$D = \frac{j_{max}^2 \cdot t_{max}}{0.1629(zFc)^2} \quad (5)$$

$$D = \frac{j_{max}^2 \cdot t_{max}}{0.2598(zFc)^2} \quad (6)$$

In these equations, D is the diffusion coefficient, z the number of charge, F the Faraday constant and c the salt concentration in the electrolyte.

The diffusion coefficient was obtained from the current-time curve of the Mg deposition on the different metal substrate at E = −1.000 V (vs. Mg/Mg^{2+}) from a solution of 0.05 M $MgCp_2$/THF (Table 4).

The validation of this value was done with the Cottrell equation (equation 7).[21,44]

$$|i| = \frac{n \cdot F \cdot A \cdot \sqrt{D}}{\sqrt{\pi} \cdot \sqrt{t}} \quad (7)$$

$$D^{1/2} = \frac{\sqrt{\pi}}{z \cdot F \cdot c} \cdot slope \quad (8)$$

Table 4. Diffusion Coefficient (in $cm^2 s^{-1}$) for several metal substrates according to the S–H Mode. $Mg(Cp)_2$ 0.05 M/THF Electrolyte. Average value is calculated based on the experiment at E = −1.000 V (vs. Mg/Mg^{2+}) for which S–H model application is valid across all the substrates.

E (Vs. Mg/Mg^{2+})/V	Cu	Ni	Al	SS
E = −1.000 V	$4.732*10^{-10}$	$1.390*10^{-10}$	$3.514*10^{-10}$	$1.000*10^{-10}$

The slope of the linear regression between the j vs. $t^{1/2}$ and equation 16 resulted in a value of $1.66 \cdot 10^{-10}\,cm^2 s^{-1}$ for the diffusion coefficient. All values are close with only a slight deviation.

Conclusions

This work shows that the halogen-free electrolyte $MgCp_2$ (Magnesocene) can be used to efficiently electrodeposit Mg on several selected current collectors namely, copper, nickel, aluminium, stainless steel. Magnesium nucleation was investigated with the Scharifker and Hills model. This model predicts a different Mg nucleation mechanism depending on the nature of the substrate and the applied potential. Thereby, inside the model boundaries, it seems that the 3D-Instantaneous mechanism is predominating for Cu, Ni, SS, while Al exhibits a more substrate and potential dependent behaviour at a $Mg(Cp)_2$ concentration of 0.05 M in THF. The results from this model were validated by SEM imaging. Further, this model can be used as an alternative way of calculating the diffusion coefficient, which is for the Magnesocene electrolyte at around $10^{-10}\,cm^2 s^{-1}$.

This work shows that investigating the nucleation behaviour of Mg on different metal substrates can result in gaining useful information, which can contribute to the topic of post-lithium batteries. Investigating additional electrolyte solutions for Mg batteries could result in a deeper understanding of the anode/electrolyte interface with different substrates and might help in designing improved electrolytes and tuned interfaces/interphases.

Experimental Section

For all experiments, materials and samples were stored, handled, and prepared in an Ar-filled glovebox (MBraun 200B). Tetrahydrofuran (THF) was dried over molecular sieves before use. The $MgCp_2$-salt (ABCR, 99.99 %, ampules under Argon) was used as received. The Cu, Al, Ni and SS substrates were ordered as foils, electrodes stamped out, and dried in a Büchi at 120 °C, at 10^{-2} bar overnight. An Mg-disk and Mg-wire were used as counter and quasi-reference electrodes, respectively. Magnesium was thoroughly polished before use to eliminate impurities on its surface and remove the native oxide layer.

For electrochemical experiments, a three electrode EL-CELL® was used. The cell was assembled using a 18 mm circular magnesium counter electrode (CE), a piece of Mg-wire as quasi-reference electrode (QRE), and different metal substrate circular electrodes (d = 18 mm) as working electrodes (WE). A glass fibre disk filled with 450 μL of electrolyte was used as separator and electrolyte reserve. The electrochemical tests were performed on a BioLogic VMP3 electrochemical workstation.

Mg-electrolyte interface was activated by a 50-cycles CV experiment at a scan rate of 10 mVs^{-1}, in the potential range $-0.500\,V < E(V\ vs.\ Mg/Mg^{2+}) < 1.200\,V$.

To investigate Mg nucleation, chronoamperometry (CA) experiments were run a selected potential values. The potential was set to the desired value and held for 190 seconds. The response current was recording with a sampling rate of 10^{-3} s and every 0.001 A. An intermediate CA experiment, setting a positive potential, was used to remove the plated magnesium. A resting period of at least 60 s at OCP was included in between the measurements. All the experiments have been run a room temperature.

Acknowledgements

The authors thank Ildiko Lüdeking and Fabian Regnet for the SEM imaging. The authors acknowledge the funding from the German Federal Ministry of Education and Research (BMBF) within projects LuCaMag (03EK3051D) and CaSaBatt (03XP0483D). This work contributes to the research performed at CELEST (Center for Electrochemical Energy Storage Ulm-Karlsruhe), and was partly funded by the German Research Foundation (DFG) under Project ID 390874152 (POLiS Cluster of Excellence). Data is available at Zenodo.[44]

Conflict of Interests

The authors declare that they have no conflict of interest.

Data Availability Statement

The data that support the findings of this study are openly available in Dataset at 10.5281/zenodo.8119805, reference number 44.

Keywords: electrodeposition · Scharifker-Hills · Magnesium batteries · aprotic electrolyte · current collectors

[1] M. Armand, J.-M. Tarascon, *Nature* **2008**, *451* (7179), 652–657.
[2] D. Larcher, J.-M. Tarascon, *Nat. Chem.* **2015**, *7* (1), 19–29.
[3] M. Marinaro, D. Bresser, E. Beyer, P. Faguy, K. Hosoi, H. Li, J. Sakovica, K. Amine, M. Wohlfahrt-Mehrens, S. Passerini, *J. Power Sources* **2020**, *459*, 228073.
[4] S. Chu, A. Majumdar, *Nature* **2012**, *488* (7411), 294–303.
[5] C. B. Bucur, *Challenges of a Rechargeable Magnesium Battery*, Cham, Springer International Publishing, **2018**.
[6] M. Winter, B. Barnett, K. Xu, *Chem. Rev.* **2018**, *118* (23), 11433–11456.

[7] A. M. Melemed, A. Khurram, B. M. Gallant, *Batteries & Supercaps* **2020**, *3* (7), 570–580.
[8] H. D. Yoo, I. Shterenberg, Y. Gofer, G. Gershinsky, N. Pour, D. Aurbach, *Energy Environ. Sci.* **2013**, *6* (8), 2265.
[9] M. Marinaro, S. Dsoke, *Nanomaterials (Basel, Switzerland)* **2022**, *12* (15) 2512.
[10] F. Maroni, S. Dongmo, C. Gauckler, M. Marinaro, M. Wohlfahrt-Mehrens, *Batteries & Supercaps* **2021**, *4* (8), 1221–1251.
[11] S. Dongmo, F. Maroni, C. Gauckler, M. Marinaro, M. Wohlfahrt-Mehrens, *J. Electrochem. Soc.* **2021**, *168* (12), 120541.
[12] J. Popovic, *Nat. Commun.* **2021**, *12* (1), 6240.
[13] J. D. Forero-Saboya, D. S. Tchitchekova, P. Johansson, M. R. Palacín, A. Ponrouch, *Adv Materials Inter* **2022**, *9 (8)*, 2101578.
[14] Y. Liang, H. Dong, D. Aurbach, Y. Yao, *Nat. Energy* **2020**, *5* (9), 646–656.
[15] Z. Liang, C. Ban, *Angew. Chem. Int. Ed.* **2021**, *60* (20), 11036–11047.
[16] J. Shi, J. Zhang, J. Guo, J. Lu, *Nanoscale Horiz.* **2020**, *5* (11), 1467–1475.
[17] C. Wei, L. Tan, Y. Zhang, Z. Wang, J. Feng, Y. Qian, *Energy Storage Mater.* **2022**, *52*, 299–319.
[18] C. Wei, L. Tan, Y. Zhang, Z. Wang, B. Xi, S. Xiong, J. Feng, *EnergyChem* **2022**, *4* (5), 100089.
[19] F. Fiesinger, D. Gaissmaier, M. van den Borg, J. Beßner, A. C. T. van Duin, T. Jacob, *ChemSusChem* **2023**, *16* (3), e202201821.
[20] F. Fiesinger, D. Gaissmaier, M. van den Borg, T. Jacob, *ChemSusChem* **2022**, *15* (14), e202200414.
[21] S. Dongmo, S. Zaubitzer, P. Schüler, S. Krieck, L. Jörissen, M. Wohlfahrt-Mehrens, M. Westerhausen, M. Marinaro, *ChemSusChem* **2020**, *13* (13), 3530–3538.
[22] S. Zaubitzer, S. Dongmo, P. Schüler, S. Krieck, F. Fiesinger, D. Gaissmaier, M. van den Borg, T. Jacob, M. Westerhausen, M. Wohlfahrt-Mehrens, M. Marinaro, *Energy Tech* **2022**, *10 (8)*, 2200440.
[23] P. Schüler, S. Sengupta, S. Zaubitzer, F. Fiesinger, S. Dongmo, H. Görls, M. Wohlfahrt-Mehrens, M. van den Borg, D. Gaissmaier, S. Krieck, M. Marinaro, T. Jacob, M. Westerhausen, *Eur J Inorg Chem* **2022**, *2022 (17)*, e202200149.
[24] R. Mohtadi, O. Tutusaus, T. S. Arthur, Z. Zhao-Karger, M. Fichtner, *Joule* **2021**, *5* (3), 581–617.
[25] R. Schwarz, M. Pejic, P. Fischer, M. Marinaro, L. Jörissen, M. Wachtler, *Angew. Chem. Int. Ed.* **2016**, *55* (48), 14958–14962.
[26] R. Davidson, A. Verma, D. Santos, F. Hao, C. D. Fincher, D. Zhao, V. Attari, P. Schofield, J. van Buskirk, A. Fraticelli-Cartagena, T. E. G. Alivio, R. Arroyave, K. Xie, M. Pharr, P. P. Mukherjee, S. Banerjee, *Mater. Horiz.* **2020**, *7* (3), 843–854.
[27] R. Davidson, A. Verma, D. Santos, F. Hao, C. Fincher, S. Xiang, J. van Buskirk, K. Xie, M. Pharr, P. P. Mukherjee, S. Banerjee, *ACS Energy Lett.* **2019**, *4* (2), 375–376.
[28] M. S. Ding, T. Diemant, R. J. Behm, S. Passerini, G. A. Giffin, *J. Electrochem. Soc.* **2018**, *165* (10), A1983–A1990.
[29] J. Eaves-Rathert, K. Moyer, M. Zohair, C. L. Pint, *Joule* **2020**, *4* (6), 1324–1336.
[30] L. C. Merrill, J. L. Schaefer, *Front. Chem.* **2019**, *7*, 194.
[31] N. LIU, L. WANG, Y. WU, L. WANG, *Int. J. Mod. Phys. B* **2009**, *23 (06n07)*, 838–842.
[32] B. Scharifker, G. Hills, *Electrochim. Acta* **1983**, *28* (7), 879–889.
[33] A. Mashreghi, H. Zare, *Curr. Appl. Phys.* **2016**, *16* (5), 599–604.
[34] G. Oskam, J. G. Long, A. Natarajan, P. C. Searson, *J. Phys. D* **1998**, *31* (16), 1927–1949.
[35] Ž. Petrović, M. Metikoš-Huković, Z. Grubač, S. Omanović, *Thin Solid Films* **2006**, *513* (1–2), 193–200.
[36] M. C. Lefebvre, B. E. Conway, *J. Electroanal. Chem.* **2000**, *480* (1–2), 34–45.
[37] M. Del, C. Aguirre, H. Núñez Coavas, L. M. Fabietti, S. E. Urreta, *J. Phys. Chem. C* **2016**, *120* (39), 22142–22154.
[38] Y.-X. Yao, J. Wan, N.-Y. Liang, C. Yan, R. Wen, Q. Zhang, *J. Am. Chem. Soc.* **2023**, *145* (14), 8001–8006.
[39] P. Jankowski, R. Schwarz, A. Randon-Vitanova, R. Younesi, M. Wachtler, P. Johansson, *Batteries & Supercaps* **2021**, *4* (8), 1335–1343.
[40] R. Schwarz, *New electrolytes and anode materials for magnesium batteries* **2018**, Dissertation. DOI. https://doi.org/10.18725/OPARU-5422.
[41] M. Paunovic, M. Schlesinger, *Fundamentals of electrochemical deposition*, **2006**, Hoboken N. J., Wiley-Interscience.
[42] B. Thirumalraj, T. T. Hagos, C.-J. Huang, M. A. Teshager, J.-H. Cheng, W.-N. Su, B.-J. Hwang, *J. Am. Chem. Soc.* **2019**, *141* (46), 18612–18623.
[43] S. Bijani, R. Schrebler, E. A. Dalchiele, M. Gabás, L. Martínez, J. R. Ramos-Barrado, *J. Phys. Chem. C* **2011**, *115* (43), 21373–21382.
[44] *Dataset.* 10.5281/zenodo.8119805.

Manuscript received: April 10, 2024
Revised manuscript received: May 22, 2024
Accepted manuscript online: June 3, 2024
Version of record online: July 10, 2024